Electronic Supplementary Material (ESI) for RSC Advances.
This journal is © The Royal Society of Chemistry 2022

Supporting Information

A Eu(III) metal–organic framework based on anthracenyl and alkynyl conjugation as a fluorescence probe for the selective monitoring of Fe^{3+} and TNP

Table of contents

Synthesis of 10-[(2-amino-4-carboxyl-phenyl)ethynyl]anthracene-9-carboxylic acid

(i)Synthesis of methyl 10-((trimethylsilyl)ethynyl)anthracene-9-carboxylate

Methyl 10-iodaanthracene-9-carboxylate (26.21 g, 0.0724 mol), copper iodide (0.328 g, 1.76 mmol) and $Pd(PPh_3)_2Cl_2$ (0.25 g, 0.36 mmol) were placed in a three-necked flask, add triethylamine (240 mL) and purged with N_2, and stir for 15 h at 60 °C. Trimethylsilylacetylene (15.36 mL, 0.109 mol) was added with a syringe, and the reaction was monitored by thin layer chromatography (TLC). The mixture was transferred to an eggplant-shaped flask, the solvent was removed under reduced pressure, dissolved with dichloromethane, then extracted with ethyl acetate. The extract was dried with anhydrous magnesium sulfate and then filtered, and the filtrate was concentrated by a rotary evaporator. The brown-yellow solid was obtained after purified by column chromatography.

(ii)Synthesis of methyl 10-ethynylanthracene-9-carboxylate

Methyl 10-((trimethylsilyl)ethynyl)anthracene-9-carboxylate (21.86 g, 65.81 mmol) was dissolved in methanol (200 mL), potassium carbonate (13.64 g, 98.72 mmol) was added, and purged with N_2, and stirred at room temperature for 4 h. The solvent was removed under reduced pressure, dissolved in dichloromethane, dried with anhydrous magnesium sulfate, and filtered. The filtrate was concentrated by a rotary evaporator, and methanol was recrystallized to obtain methyl 10-ethynylanthracene-9-carboxylate.

(iii)Synthesis of 10-[(2-amino-4-(methoxycarbonyl)phenyl)ethynyl]anthracene-9-carboxylate

Methyl 3-amino-4-iodobenzoate (2.77g, 10 mmol), $Pd(PPh_3)_2Cl_2$ (0.35 g, 0.5 mmol) and copper iodide (0.19 g, 1 mmol) were dissolved in triethylamine in a three-necked flask, then added triethylamine solution of methyl 10-((trimethylsilyl)ethynyl)anthracene-9-carboxylate, and purged with N_2, stirred at 90 °C for 24 h. The reaction was monitored by TLC. The mixture was transferred to an eggplant-shaped flask, the solvent was removed under reduced pressure, dissolved with dichloromethane, then extracted with ethyl acetate. The extract was dried with anhydrous magnesium sulfate and then filtered, and the filtrate was concentrated by a rotary evaporator. The solid was obtained after purified by column chromatography.

(iv)Synthesis of 10-[(2-amino-4-carboxyl-phenyl)ethynyl]anthracene-9-carboxylic acid

Dissolved the above-mentioned purified product in a mixture solution of THF and aqueous, added NaOH with constant stirring, acidified with 2 M hydrochloric acid, and filter to obtain 10-[(2-amino-4-carboxyl-phenyl)ethynyl]anthracene-9-carboxylic acid. The ^{1}H NMR spectrum of 10-[(2-amino-4-carboxyl-phenyl)ethynyl]anthracene-9-carboxylic acid is in Fig. S1.

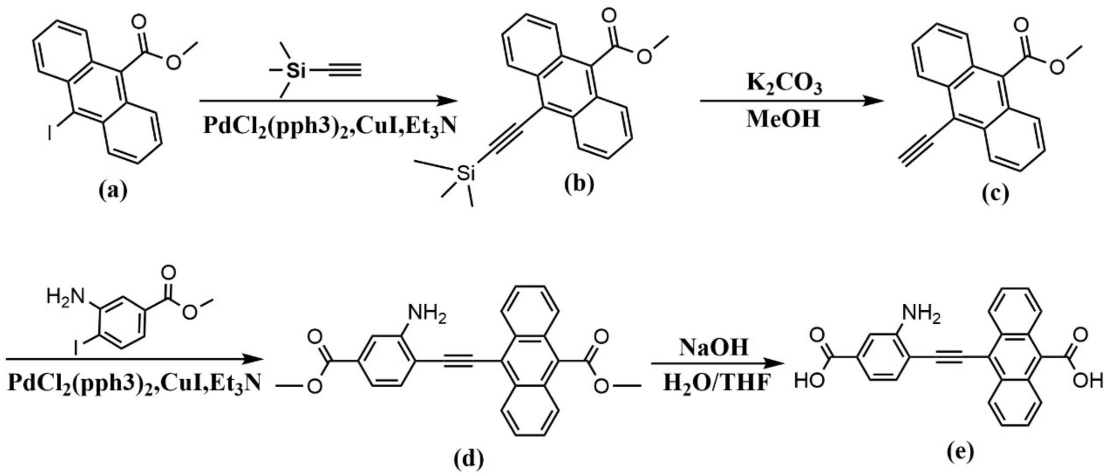

Scheme S1. Synthesis of 10-[(2-amino-4-carboxyl-phenyl)ethynyl]anthracene-9-carboxylic acid.

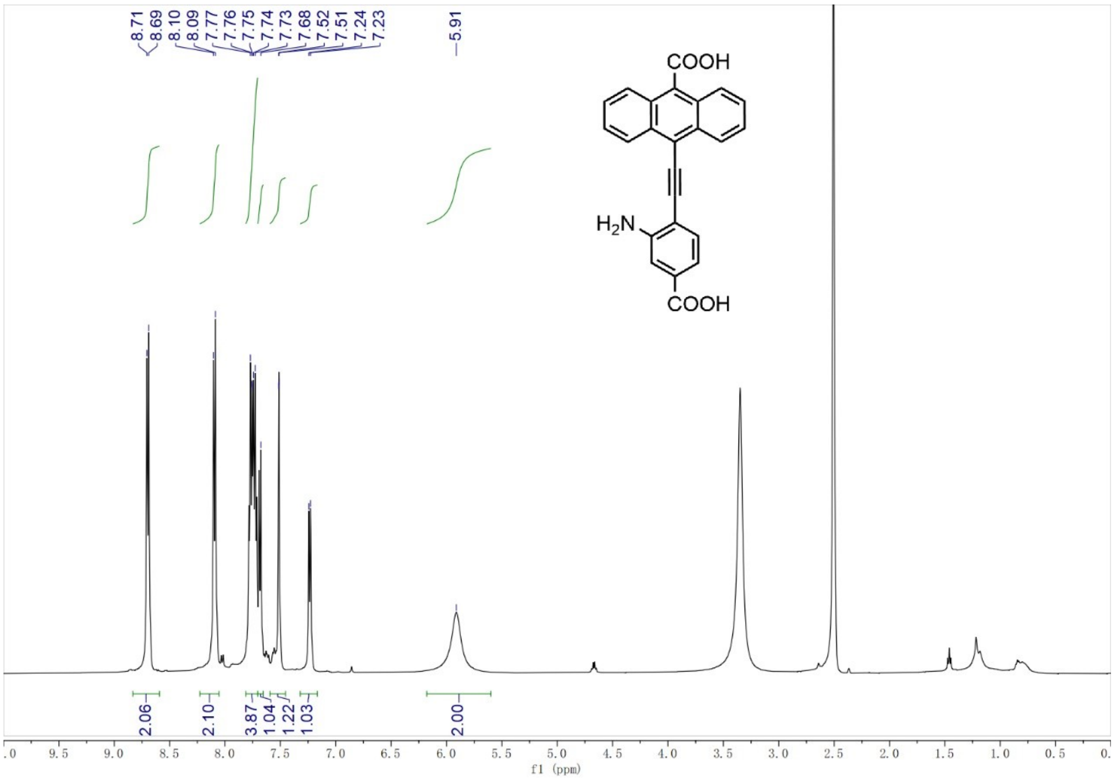

Fig. S1. ^{1}H NMR spectrum for for 10-[(2-amino-4-carboxyl-phenyl)ethynyl]anthracene-9-carboxylic acid

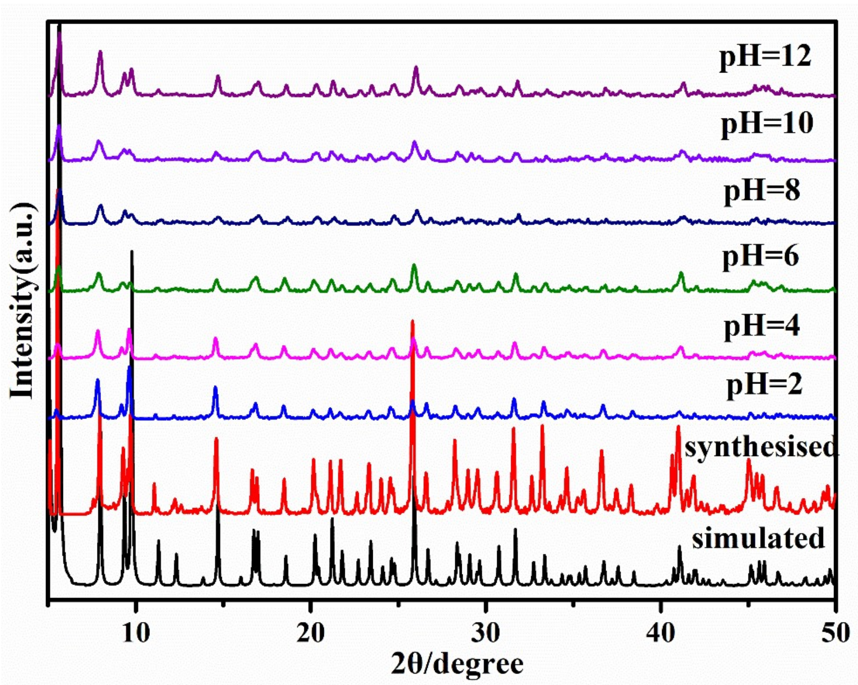

Fig. S2. PXRD of Eu-MOF after treatment in pH = 2-12 DMF solution.

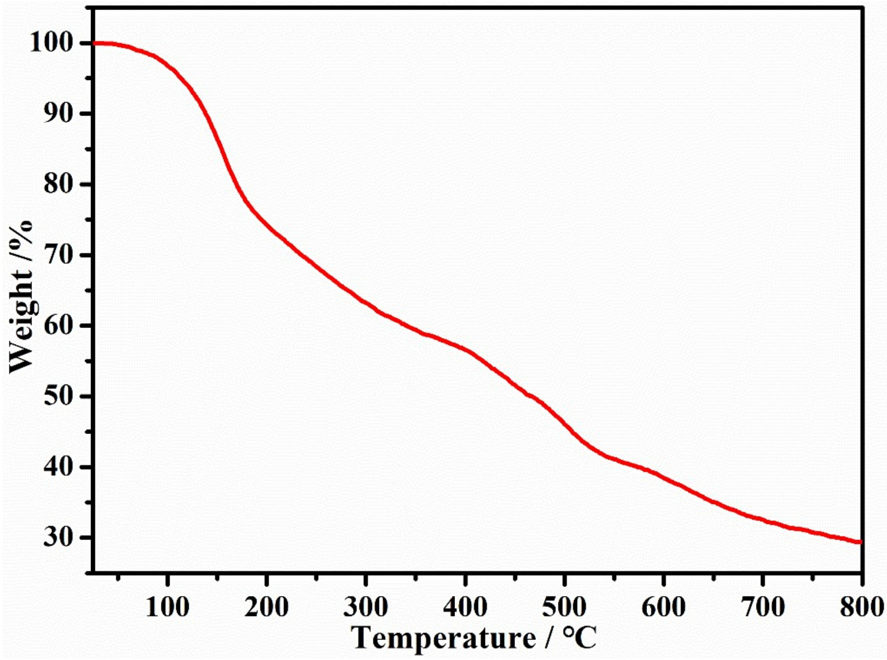

Fig. S3. The TGA curves of Eu-MOF.

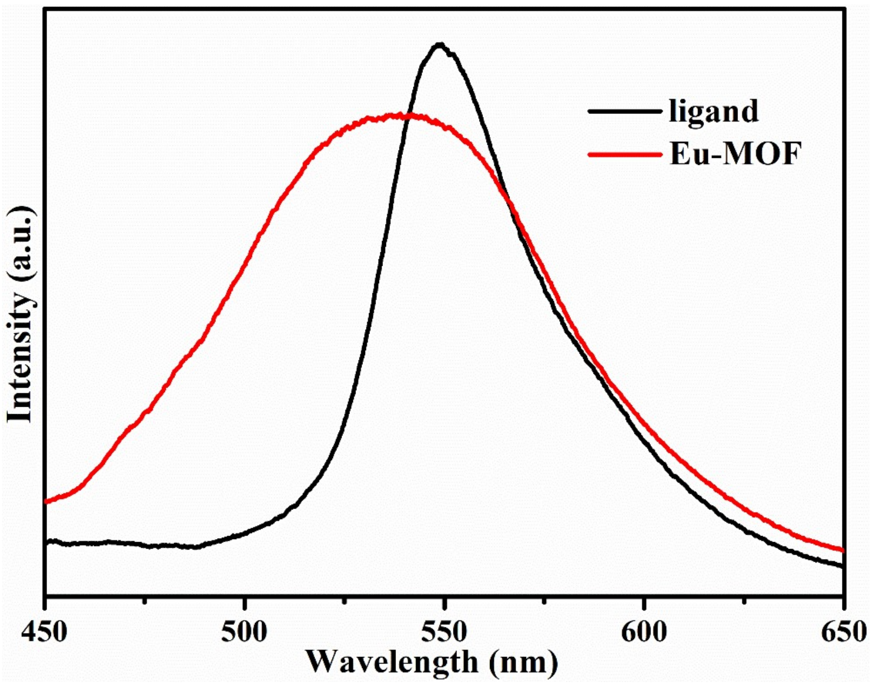

Fig. S4. The solid emission spectra of ligand and Eu-MOF.

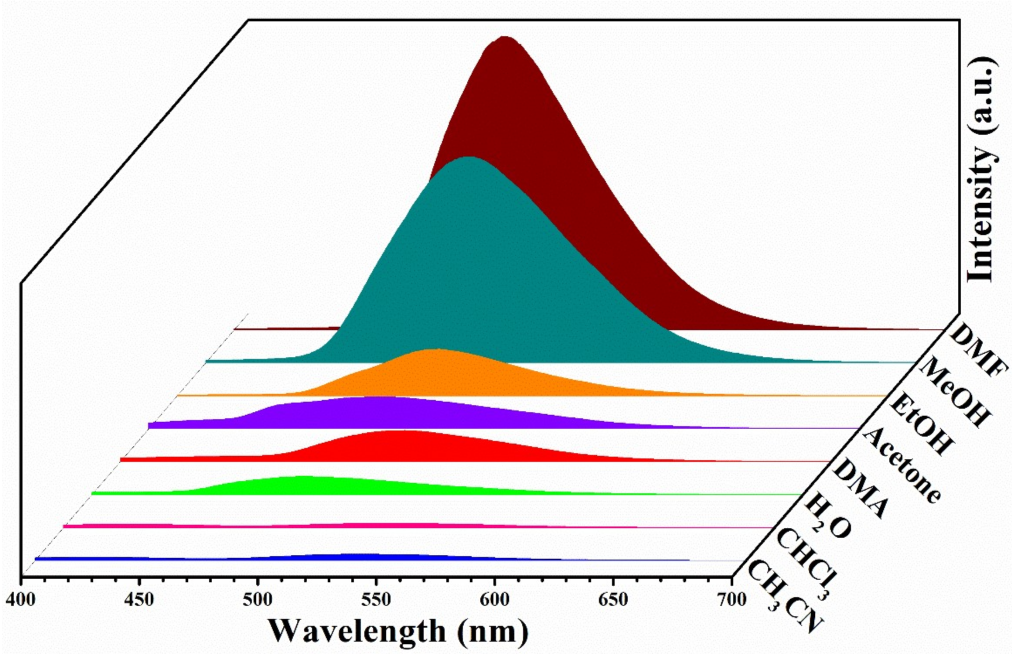

Fig. S5. Luminescence spectra of Eu-MOF in different solvents.

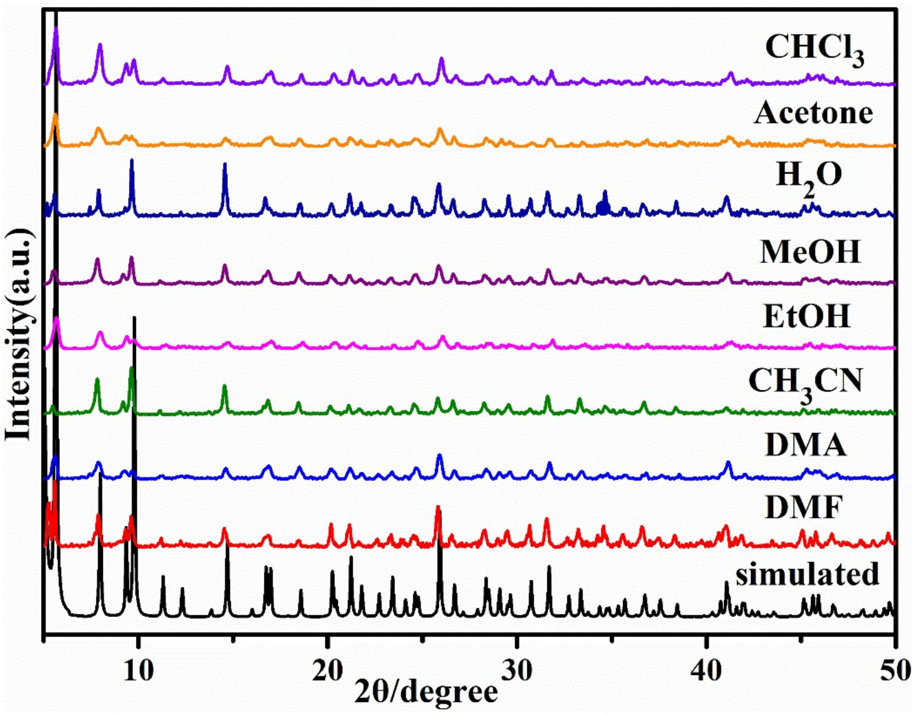

Fig. S6. PXRD of Eu-MOF in different solvents.

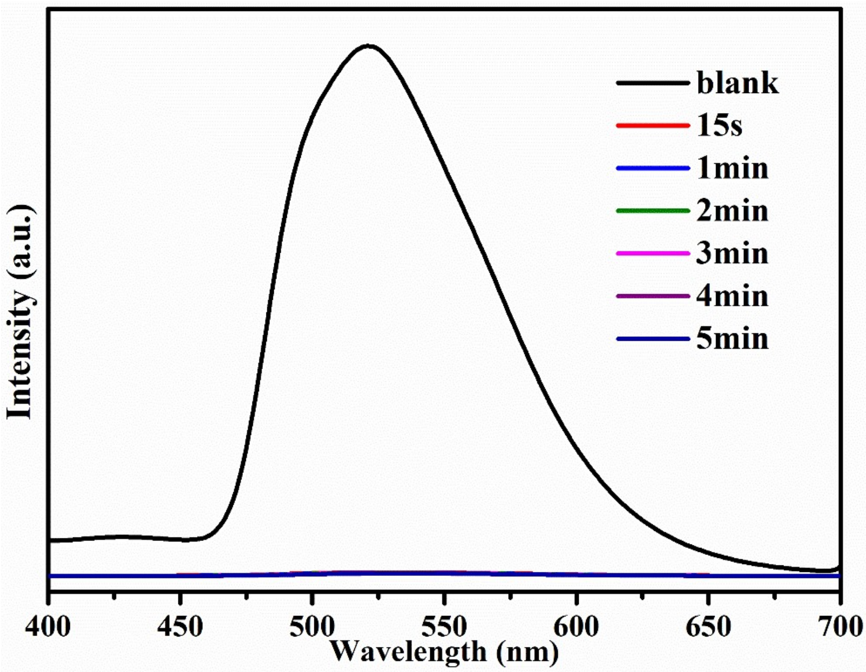

Fig. S7a. Time-dependent fluorescence spectrum after adding Fe^{3+} (10^{-3}M).

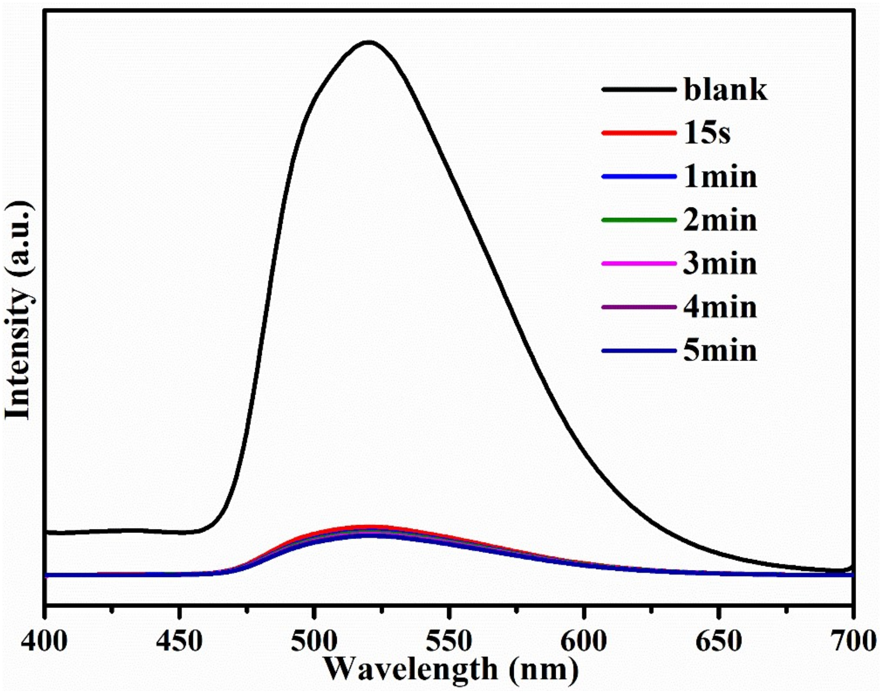

Fig. S7b. Time-dependent fluorescence spectrum after adding TNP (10^{-4}M).

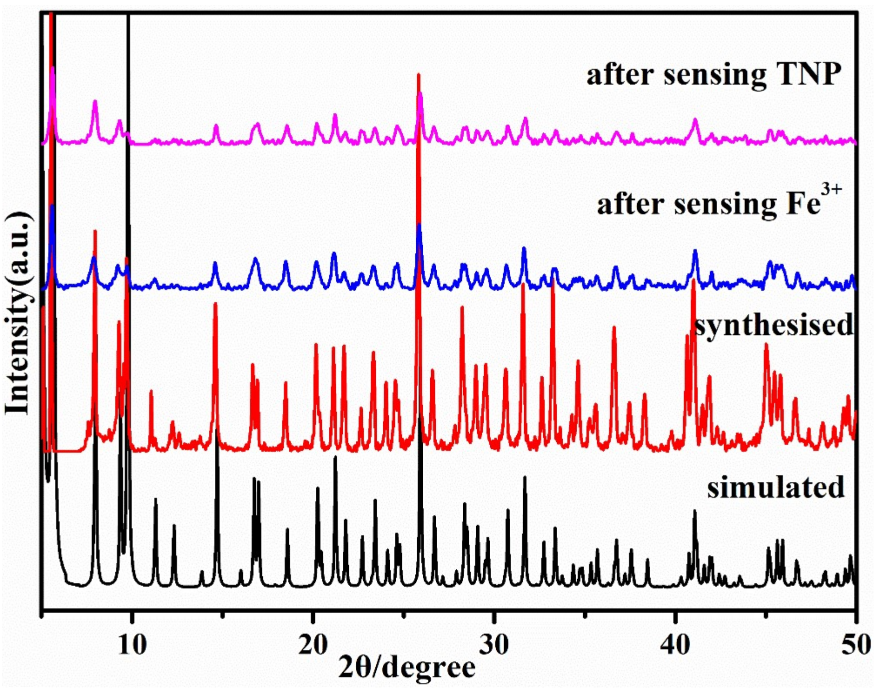

Fig. S8. PXRD of Eu-MOF after detection Fe^{3+} and TNP.

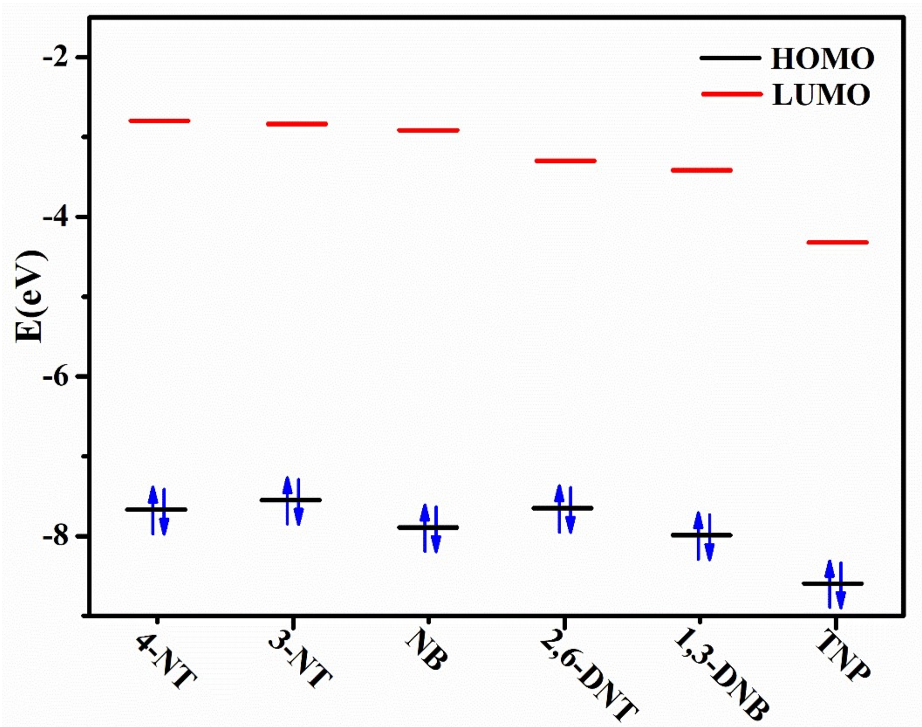

Fig. S9. HOMO and LUMO energy level of NAEs.

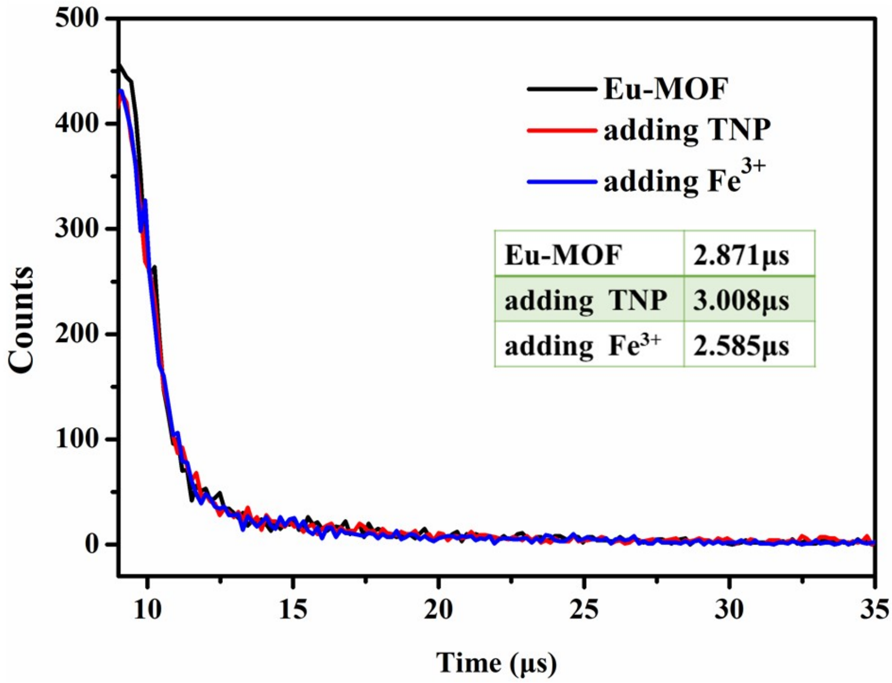

Fig. S10. The fluorescence lifetime of Eu-MOF, after adding Fe^{3+} and TNP .

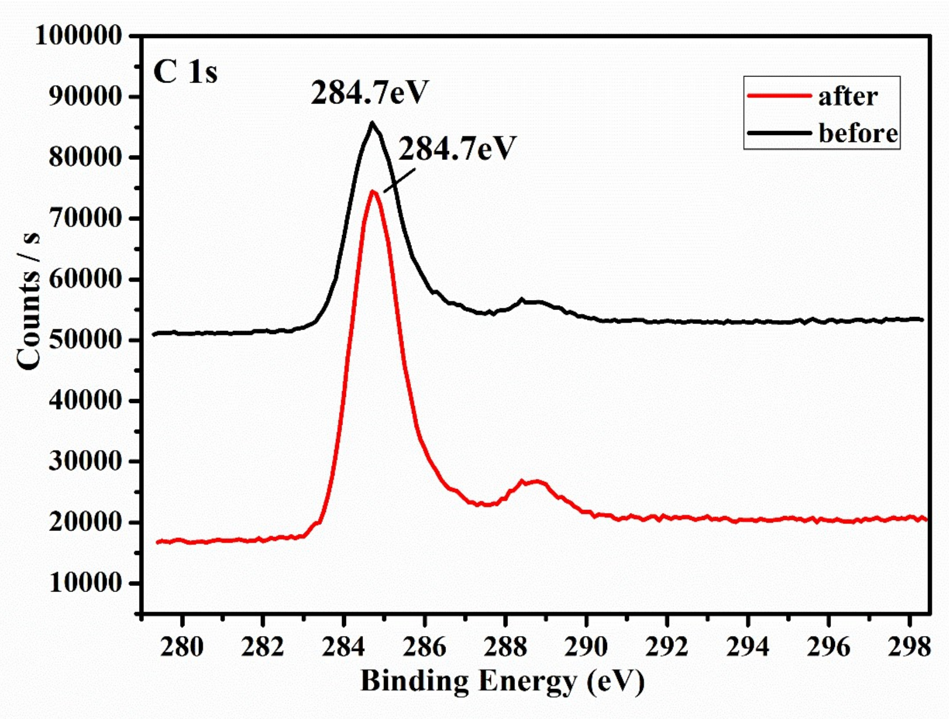

Fig. S11. XPS spectra of Eu-MOF before and after immersing in Fe^{3+}

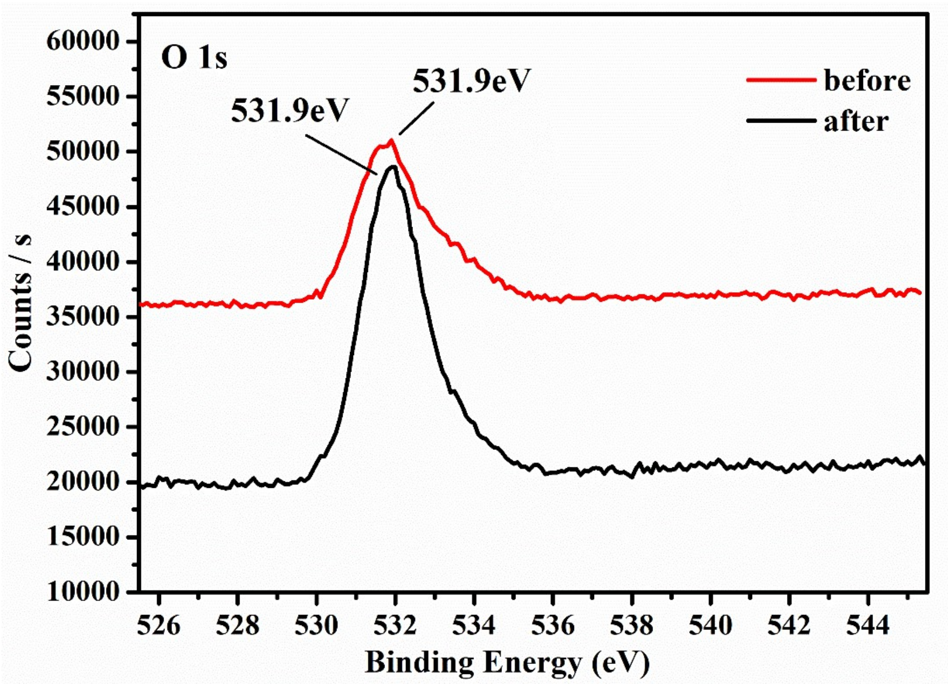

Fig. S12. XPS spectra of Eu-MOF before and after immersing in Fe^{3+}

Table S1. Selected bond lengths (Å) and angles (°) for Eu-MOF

Bond lengths			
Eu1—Eu11	3.9036(13)	Eu1—O16	2.361(8)
Eu1—Eu12	3.9036(13)	Eu1—O28	2.331(2)
Eu1—Eu13	3.9036(13)	Eu1—O27	2.331(2)
Eu1—O14	2.360(8)	Eu1—O21	2.331(2)
Eu1—O1	2.362(8)	Eu1—O2	2.331(2)
Eu1—O15	2.361(8)	Eu1—O3	2.86(4)
Bond angles			
Eu11—Eu1—Eu12	60	O27—Eu1—Eu11	33.13(9)
Eu12—Eu1—Eu13	90	O2—Eu1—Eu11	85.93(19)
Eu11—Eu1—Eu13	60	O27—Eu1—O16	76.2(2)
O14—Eu1—Eu13	158.7(2)	O28—Eu1—O16	138.99(13)
O1—Eu1—Eu11	106.53(15)	O27—Eu1—O14	138.99(13)
O15—Eu1—Eu12	106.53(15)	O28—Eu1—O14	76.2(2)
O15—Eu1—Eu11	158.7(2)	O22—Eu1—O1	138.99(13)
O1—Eu1—Eu13	68.7(2)	O28—Eu1—O15	76.2(2)
O14—Eu1—Eu12	68.7(2)	O28—Eu1—O1	138.99(13)
O14—Eu1—Eu11	106.53(15)	O27—Eu1—O1	76.2(2)
O16—Eu1—Eu13	106.53(15)	O2—Eu1—O16	138.99(13)
O16—Eu1—Eu12	106.53(15)	O27—Eu1—O15	138.99(13)
O1—Eu1—Eu12	158.7(2)	O22—Eu1—O14	76.2(2)
O16—Eu1—Eu11	68.7(2)	O2—Eu1—O15	76.2(2)
O15—Eu1—Eu13	106.53(15)	O22—Eu1—O16	76.2(2)
O15—Eu1—O1	80.68(17)	O22—Eu1—O15	138.99(13)
O15—Eu1—O16	132.5(5)	O2—Eu1—O1	76.2(2)
O14—Eu1—O1	132.5(5)	O2—Eu1—O14	138.99(13)
O16—Eu1—O14	80.68(17)	O22—Eu1—O2	100.1(4)
O15—Eu1—O14	80.68(17)	O22—Eu1—O27	65.6(2)
O16—Eu1—O1	80.68(17)	O27—Eu1—O2	65.6(2)
O14—Eu1—O3	66.3(2)	O22—Eu1—O28	65.6(2)
O1—Eu1—O3	66.3(2)	O28—Eu1—O27	100.1(4)
O16—Eu1—O3	66.3(2)	O28—Eu1—O2	65.6(2)
O15—Eu1—O3	66.3(2)	O22—Eu1—O3	130.0(2)
O2—Eu1—Eu13	33.13(9)	O27—Eu1—O3	130.0(2)
O27—Eu1—Eu12	85.93(19)	O2—Eu1—O3	130.0(2)
O2—Eu1—Eu12	85.93(19)	O28—Eu1—O3	130.0(2)
O22—Eu1—Eu11	33.13(9)	O3—Eu1—Eu11	135
O27—Eu1—Eu13	33.13(9)	O3—Eu1—Eu13	135
O28—Eu1—Eu13	85.93(19)	O3—Eu1—Eu12	135
O22—Eu1—Eu13	85.93(19)	C1—O1—Eu1	136.5(10)
O22—Eu1—Eu12	33.13(9)	Eu18—O2—Eu13	113.73(18)
O28—Eu1—Eu12	33.13(9)	Eu1—O2—Eu18	113.73(18)
O28—Eu1—Eu11	85.93(19)	Eu1—O2—Eu13	113.73(18)

Table S2. A comparison of MOFs-based luminescent sensors for detection Fe^{3+}.

sensors based on MOFs	*Ksv* (M^{-1})	LOD	Ref
Eu-MOF	5.06×10^5	0.51μM	thiswork
Zn-MOF	1.326×10^4	0.882μM	1
$[H(H_2O)_8][DyZn_4(imdc)_4(im)_4]$	9.29×10^5	—	2
$[Zn_2Na_2(TPHC)(4,4\text{-}Bipy)(DMF)]\cdot 8H_2O$	5.77×10^4	6.4μM	3
MOF-808-Tb	3.1×10^4	—	4
$[Eu_2(HICA)(BTEC)(H_2O)_2]_n$	2.028×10^4	—	5
$Y_{10}(C_8H_4O_4)_6(CO_3)_3(OH)_{12}$	1.905×10^4	12.7μM	6
Eu-MOF/EDTA-NiAl-CLDH–M	1.3×10^4	0.15μM	7

Table S3. A comparison of MOFs-based luminescent sensors for detection TNP.

sensors based on MOFs	*Ksv* (M^{-1})	LOD	Ref
Eu-MOF	1.92×10^4	1.93×10^{-6}M	thiswork
$[Cd(3\text{-}bpd)(N(CN)_2)_2]_n$	7.16×10^4	6×10^{-5} M	8
TMU-34	4.9×10^4	8.1×10^{-6} M	9
$\{[Cd_3(bmipia)_2]\cdot 10DMF\cdot 5H_2O\}n$	3.82×10^4	—	10
EuL	1.36×10^3	1×10^{-5}M	11
TbL	4.995×10^3	5×10^{-6}M	11
$[\{Zn(BINDI)_{0.5}(bpe)_{0.5}\}\cdot 3H_2O]_n$	1.29×10^4	1.5ppm	12

Table S4. HOMO and LUMO energy of NAEs at B3LYP/6-31G* level of theory.

NAEs	HOMO (eV)	LUMO (eV)	Band gap (eV)
4-NT	-7.65502	-2.79225	4.86277
3-NT	-7.55031	-2.83893	4.71137
NB	-7.88778	-2.91263	4.97515
2,6-DNT	-7.6448	-3.2877	4.3571
1,3-DNB	-7.9855	-3.4311	4.5544
TNP	-8.59516	-4.32093	4.27423

Reference

1. B. B. Rath and J. J. Vittal, *Inorganic Chemistry*, 2020, **59**, 8818-8826.
2. Y.-F. Li, D. Wang, Z. Liao, Y. Kang, W.-H. Ding, X.-J. Zheng and L.-P. Jin, *Journal of Materials Chemistry C*, 2016, **4**, 4211-4217.
3. C. Yu, X. Sun, L. Zou, G. Li, L. Zhang and Y. Liu, *Inorganic Chemistry*, 2019, **58**, 4026-4032.
4. J. Zhang, S. B. Peh, J. Wang, Y. Du, S. Xi, J. Dong, A. Karmakar, Y. Ying, Y. Wang and D.

Zhao, *Chemical Communications*, 2019, **55**, 4727-4730.

5. H. Yu, M. Fan, Q. Liu, Z. Su, X. Li, Q. Pan and X. Hu, *Inorganic Chemistry*, 2020, **59**, 2005-2010.
6. W. Chen, L. Li, X.-X. Li, L.-D. Lin, G. Wang, Z. Zhang, L. Li and Y. Yu, *Crystal Growth & Design*, 2019, **19**, 4754-4764.
7. W. Yang, J. Li, Z. Xu, J. Yang, Y. Liu and L. Liu, *Journal of Materials Chemistry C*, 2019, **7**, 10297-10308.
8. S. Halder, P. Ghosh, C. Rizzoli, P. Banerjee and P. Roy, *Polyhedron*, 2017, **123**, 217-225.
9. S. A. A. Razavi, A. Morsali and M. Piroozzadeh, *Inorganic Chemistry*, 2022, **61**, 7820-7834.
10. M.-Y. Zhang, R.-D. Dai, B.-J. Li, T.-X. Hang, J.-X. Xie, J. Lü and X.-D. Zhu, *Crystal Growth & Design*, 2020, **20**, 1373-1377.
11. W. Liu, X. Huang, C. Chen, C. Xu, J. Ma, L. Yang, W. Wang, W. Dou and W. Liu, *Chemistry – A European Journal*, 2019, **25**, 1090-1097.
12. S. S. Dhankhar, N. Sharma and C. M. Nagaraja, *Inorganic Chemistry Frontiers*, 2019, **6**, 1058-1067.